Published in final edited form as:
Nano Lett. 2009 May ; 9(5): 2160–2166. doi:10.1021/nl9007425.

Influence of Transient Environmental Photothermal Effects on Optical Scattering by Gold Nanoparticles

Ekaterina Y. Lukianova-Hleb[†] and **Dmitri O. Lapotko**[*,†,‡]

[†] A. V. Lykov Heat and Mass Transfer Institute, 15 P. Brovka Street, Minsk, 220072, Belarus

[‡] Rice University, 6100 Main Street, Texas 77005

Abstract

Transient photothermal phenomena in the environment of light-absorbing plasmonic nanoparticles, heating and evaporation, were shown to influence the optical scattering efficacy of such nanoparticles, when they absorb and scatter the light. The heating of the environment suppresses the optical scattering, while the evaporation enhances the scattering by the nanoparticles. These opposite effects have transient, local, and thermal nature and significantly (more than 10 times) influence the optical contrast of the nanoparticles as shown for gold spheres in water.

The superior optical scattering properties of gold and other plasmonic nanoparticles (NP) provided significant advances in the development of imaging methods.[1–8] The plasmon mechanism that is responsible for the scattering also provides photothermal effects allowing us to use the NPs as efficient heat sources.[5,9–14] In many cases optical scattering and photothermal processes act simultaneously, because the plasmon mechanism splits the incident optical energy into a scattered and absorbed components. Therefore, optical scattering may involve concurrent photothermal effects in an NP and around it. It was found that the plasmon properties of gold NPs (including the scattering cross-section) depend on the temperature and phase state of NPs and thus are influenced by the photothermal effects that act in the NPs.[15–19] We have hypothesized that the photothermal (PT) phenomena in the NP nanoenvironment (a transient thermal field[13,14,20] and evaporation[9,21–23] due to heat transfer from laser-heated NPs) may also influence the optical scattering by NPs, because the incident and scattered optical radiations propagate through the medium with the temperature-dependent refractive index. Until recently the studies of the optical scattering by NPs were focused on the properties of NPs themselves, and on the chemical, biological, and structural properties of the environment[24,25] and did not directly allow for the influence of the environmental photothermal (PT) effects. Since the major advantages of gold NPs as optical probes are the high sensitivity and specificity of the imaging and because NPs are always surrounded by some medium, the environmental thermal effects may be an important optical factor.

In this work, we have experimentally analyzed the influence of the gold NP-induced heating and evaporation of the medium around NPs (water) on the efficacy of optical scattering by individual gold spheres of 90 nm (no. 10-A-100, Nanopartz, Salt Lake City, UT) and 250 nm (no. 790128–010, Corpuscular Inc., NY). The concentration of the NPs was adjusted to 3.8×10^8/ml so to provide sufficient spatial separation between them (the average calculated distance based upon this concentration was 14 μm). Also the average distance was experimentally verified by using the images of the NPs that were obtained with the optical side scattering method (see below). Additionally the clusters of the same NPs were prepared by adding 40%

* To whom correspondence should be addressed. dmitri.lapotko@rice.edu.

volume of an acetone into the suspension of NPs and resuspending the clusters in water to adjust their concentration to that of the single NPs. Optical extinction spectra of the samples were obtained with spectrophotometer (USB 650 Red Tide, Ocean Optics, Inc., Dunedin, FL). The samples were prepared on the microscope slides as 10 μm thick layers of the NP water suspensions confined between microscope slide glass and the coverslip glass. The gap between the glasses was provided by adding into NP suspension 10 μm microspheres (no. FP-10052–2, Spherotech Inc., Lake Forest, IL) that separated the two glasses.

The PT heating of gold NPs occurs within a picosecond after an NP is exposed to a short pulse.[13] The heating of the NP environment takes longer time and includes thermal diffusion from the NP surface into the surrounding water and spatial and temporal evolution of the temperature field in water, including its possible evaporation (bubble generation). To make the spatial scale of the secondary PT phenomena comparable to the size of NPs, we have chosen the duration of the optical exposure of samples to be about 10^{-10} to 10^{-9} s. This time is 2 orders of magnitude longer than the time required for initial thermalization of the NPs and also is shorter than the thermal relaxation time for the NPs in water. By using the Fourier model of heat transfer,[20] the thermal relaxation times (τ) were estimated to be 4.8 ns for 250 nm gold spheres and 0.6 ns for 90 nm gold spheres as $\tau = \tau^2/24a$, where r is the radius of a gold sphere and a is the thermal diffusivity of water. Therefore, we may assume that the thermal energy is generated in the NPs during absorption of a pump laser pulse and then is transferred to the environment. The spatial scale of the secondary PT phenomena in water is estimated by the thermal radius ($r_t = (24at_p)^{1/2}$, where t_p is the laser pulse duration) and is approximately 40 nm (when the NP-induced water temperature is below the evaporation threshold) and by the maximal diameter of the vapor bubble (when the NP-induced water temperature is above the evaporation threshold). Therefore, only the local nanoenvironment of NPs is thermally influenced by the absorption of a pump pulse by them, and the induced environmental thermal inhomogeneities are of transient nature. The temperature gradients (as well as the vapor bubble surface) create certain gradients of the optical refractive index, and therefore they influence the optical radiation through the scattering, diffraction, and refraction mechanisms (depending upon their spatial scale), while the optical properties of the bulk medium remain unchanged and thus do not influence the process of optical scattering by NPs.

The optical excitation of NPs was realized at a wavelength of 532 nm, which was close to the maxima of optical absorbance of the utilized gold spheres, and with a single 500 ps laser pulse generated by a microlaser (STA-01SH, Standa Ltd., Vilnius, Lithuania). A laser beam was focused into a 6 μm spot (Figure 1), and its fluence at the sample plane was determined by monitoring the incident energy (PE10-SH, Ophir Optonics, Ltd., Israel) and the laser spot area (measured by imaging the spot by a Luka-S CCD camera, Andor Technology, Northern Ireland). To study the optical scattering, we have illuminated a sample by a single 500 ps probe laser pulse directed to the sample at an angle of 85°. This provided the side-scattering conditions for the NPs. The combination of a probe pulse wavelength of 690 nm (which is relatively separated from the spectral region of maximal plasmon absorbance by NPs) and of a pulse fluence (below 0.2 mJ/cm^2) prevented significant PT effects in NPs that might have been caused by the absorption of the probe pulse. Although an increased diameter and clusterization of NPs red shift their plasmon resonances, the absorbance at 690 nm is much lower than that at 532 nm. The probe pulse was produced by a pumping dye laser (custom-made) with the microlaser described above and by delaying the probe pulse relative to the pump pulse (532 nm) for 0.5, 1.5, 2.5, and 9 ns in order to study the scattering at different temporal stages of heat transfer from the NPs to the environment. Pulsed probe irradiation has allowed a time-resolved imaging of the NPs. The light scattered by the NPs was collected by a 60× objective (n.a. 0.85) and was imaged by the above-mentioned CCD camera.

A quantitative analysis of the scattering efficacy of an individual NP was performed using the coefficient K_{sc} as a relative scattering amplitude:

$$K_{sc} = \frac{I_t - I_{b1}}{I_0 - I_b}$$

where I_b is the averaged pixel image amplitude for the background without the pump pulse, I_{b1} is the averaged pixel image amplitude for the background with the pump pulse, I_0 is the pixel image amplitude in the center of the NP image obtained with the probe pulse and without exposure of the NP to the pump pulse, and I_t is the pixel image amplitude in the center of the NP image obtained with the probe pulse with a delay t after the exposure of the NP to the single pump laser pulse of specific fluence ε. Photothermally induced alteration of optical scattering would cause a deviation of the K_{sc} value from 1.

The thermal state of the medium around NPs was independently monitored by collinearly focusing a low power continuous probe laser at 633 nm into a sample (Figure 1). Local heating and evaporation of water around NPs was detected through a shape-specific time response signal by monitoring the axial intensity of the continuous probe beam after the sample and by a high-speed photodetector (PDA10A, Thorlabs Inc., Newton, NJ). This method is known as the “thermal lens” technique, which was described by us in detail previously.[26] The thermal lens method also allowed us to verify the generation of vapor bubbles around NPs and to measure the bubble lifetime that characterizes a maximal diameter of a vapor bubble. The samples were studied on an experimental setup that included the above-named laser sources and an inverted optical microscope (Nikon Diaphot 200, Nikon Instruments Inc., Melville, NY), which also was described in detail by us previously.[27]

The optical scattering by gold NPs has been analyzed as a function of several parameters: NP diameter (90 and 250 nm), aggregation state (single separated NP and clusters of several aggregated NPs), pump laser pulse fluence, and the time delay between the pump and probe pulses. The thermal response of an NP suspension has been independently monitored by registering its time-response by an additional continuous probe beam (633 nm) that illuminated the area of the sample exposed to the pump pulse. The pulsed optical side-scattering images of gold NPs and their clusters are shown in Figure 2a,e. This imaging mode also allowed manual positioning of a specific single NP into the center of the pump laser beam and verified spatial separation of NPs. Application of the single broad pump pulse at 532 nm (the wavelength corresponds to the absorbance peak of gold spheres) significantly changed the scattering patterns (Figure 2b,f): at a low pump fluence the scattering image pixel amplitude decreased by several times for one object, while at a higher pump fluence (in the center of laser beam) it significantly increased for another object (from 1.5 to almost 10 times). The different levels of the pump fluence during simultaneous irradiation of two objects (shown in Figure 2a,e) by one broad pump beam were provided by the spatial distribution (profile) of the pump beam fluence (curve 3 in Figure 2c,g): it was 2–3 times higher at the side of the first object relative to the pump fluence level at the side of the second object.

The discovered amplification/bleaching phenomena were reproducible for the same NPs, and the scattering pixel image amplitudes of specific NPs did not alter after their exposure to several (up to 50) pump pulses. Therefore, we assumed no photo or thermal damage to the NPs during their excitation by pump laser pulses. The detected transient change in the optical contrast (measured as a ratio of the image pixel amplitudes for the two objects) was quite dramatic due to the bleaching of the scattering around one NP and the amplification of the scattering around the other NP. For 250 nm NPs, it changed from initial 1:1 (Figure 2a,c, profile 1, scattering by

two identical NPs) to 5.4 at 9 ns delay after exposure of the same pair of NPs to a single pump laser pulse (Figure 2b,c, profile 2). Another sample representing a pair of single 90 nm NPs and a cluster of 90 nm NPs has yielded an increase in the optical contrast from 1.5 (Figure 2e,g, profile 1) when measured without a pump pulse to 26.5:1 at 9 ns delay after exposure of the NPs to a single pump laser pulse (Figure 2f,g, profile 2). This pump laser-induced change in the optical contrast correlated with different levels of the pump laser fluence (profile 3), as can be seen from Figure 2c,g.

To understand the mechanism of the discovered bleaching/amplification phenomena, we analyzed a coefficient K_{sc} (which represents a relative change in the scattering image pixel amplitudes) as a function of the pump laser fluence ε and the probe-pump time delay t. We also correlated integral time responses (Figure 2) of NP suspensions (obtained simultaneously with the exposure of the NPs to a pump pulse) with the scattering coefficients K_{sc}. The pump pulse-induced bleaching effect ($K_{sc} < 1$) was found to be associated with relatively low pump fluences for all time delays (0.5, 1.5, 2.5, and 9 ns). Also, the bleaching effect correlated with the heating–cooling type of the time-response of a NP suspension (Figure 3a) for all types of the samples studied (90 nm and 250 nm NPs and clusters of 90 nm NPs). The time-response in Figure 3a is typical of pulsed laser-induced heating of the environment (sharp front) followed by much slower cooling of the medium due to thermal diffusion (long tail in Figure 3a) with the characteristic cooling time being 20–25 ns, as estimated from the tail length. This cooling time is much longer than the cooling time for the NPs (0.6 and 4.8 ns for the 90 and 250 nm, respectively) and therefore can be attributed only to the secondary heating and cooling of the water environment by the laser-heated NPs.

The pump pulse-induced amplification of optical scattering was detected at a higher pump laser fluence and, also, the amplification effect detected was always accompanied by a completely different time-response (Figure 3b). This type of the time-response assumes the generation of a vapor bubble around an NP and shows the bubble expansion and collapse curves (as was found previously[27,28]). The bubble-type response has the opposite sign to the heating–cooling response (Figure 3a), which indicates that these two thermal processes have an opposite optical effect on the continuous probe beam too. We have measured the duration of the bubble-specific response to characterize the bubble lifetime, which is approximately proportional to a maximal diameter of a bubble.[29–31] The duration of the laser-induced bubbles around NPs was found to be in the range from 10 to 100 ns; such short lifetimes correspond to nano- and micrometer maximal diameters of the pump pulse-induced bubbles. The generation of a bubble around an NP may explain the discovered effect of optical amplification: the vapor–liquid border (surface of the bubble) increases the gradient of the refractive index around an NP (relative to water) and acts as a scatterer instead of (or in addition to) the NP, and moreover an expanding bubble increases the diameter of the scattering object (relative to the NP diameter), thus additionally increasing the optical scattering. We have recently studied the influence of the NP-generated bubbles on the optical scattering in living cells[32] and have demonstrated (experimentally and theoretically) that the NP-generated vapor bubbles may amplify the optical scattering amplitude by several orders of magnitude (relative to the amplitude of the scattering by NPs).

On the basis of the above results, we conclude that the photothermal laser-induced heating of an NP influences its optical scattering efficacy by altering the thermal and consequently the optical properties of the NP nanoenvironment. Specific effect of the pump laser pulse on optical scattering (bleaching or amplification) depends upon the type of the thermal process in the NP environment (heating or evaporation), which in turn depends upon the thermal energy being generated by the NP during absorption of a pump laser pulse.

As the next step, we studied in detail the influence of the pump pulse fluence on the optical scattering at different time delays of the probe pulse (Figure 4). Applied time delays were

shorter and longer than the characteristic cooling times for the NPs (0.6 ns for 90 nm NPs; 4.8 ns for 250 nm NPs): 0.5, 1.5, 2.5, and 9 ns. The relative scattering amplitudes K_{sc} obtained (Figure 4) were plotted together with the curves for the bubble generation probability (PRB) calculated independently as the probability of the bubble-specific time-response. This parameter characterizes the probability of the PTB generation in a specific sample and for a specific fluence of the pump pulse. The PRB was measured as a ratio of the number of PTB-positive events (as detected by PTB-specific time responses for each single exposure of the sample to a pump pulse) to the total number of events. We have found that the relative scattering amplitude K_{sc} almost linearly decreases (bleaches) with the pulse fluence when no bubbles were generated ($K_{sc} < 1$), and also that an increase in the time delay of a probe laser pulse increased the bleaching effect (Figure 5a).

At the probe pulse delay times longer than the cooling time of an NP (0.6 ns for 90 nm NPs and 4.8 ns for 250 nm NPs) the temperatures of the NP and its environment become close, and these temperatures are much lower than the initial laser-induced temperature of the NP, and the heated volume significantly exceeds the volume of the NP. At the time stages that correspond to the 9 ns delay, the heated volume is mainly associated with the environment, rather than with the NP, and hence the properties of the environment become responsible for the transient optical behavior of the NP–environment system. Thus, the environment, not the NP, causes the observed bleaching of the optical scattering. Heating of the NP environment creates local density gradients and hence the transient gradients of the refractive index. However, the spatial scale of the heated NP environment remains lower than the wavelength of the probe beam. Therefore, the induced gradients of the refractive index would scatter the propagating light, and their scattering power can be expressed in terms of the Mie theory.[33] The higher the initial laser-induced temperature of the NP, the higher will be the temperature of the environment and the lower its refractive index. As a result, the intensity of an incident probe beam on the NP surface will be decreased due to its scattering by the transient gradients of the refractive index of the medium (environment) as a probe beam approaches the NP, and the intensity of the probe beam scattered by the NP will also be decreased as it propagates to the detector and through the heated environment. The described above mechanism of "photothermal" scattering influences both incident and scattered probe beams and may explain observed bleaching effect. Also, the decrease in the refractive index of the environment was shown to decrease the scattering cross section of gold NPs; for example, the decrease in the refractive index of the NP environment from 1.3 to 1.2 lowered the scattering cross-section almost by half for 30 nm gold NPs, as estimated by the Rayleigh theory.[34] These two mechanisms may act independently and thus may cause the observed decrease in the optical scattering by gold NPs due to the photothermal heating of the NP environment.

The scattering behavior changed in principle when the pump laser fluence exceeded the specific threshold and indicated a steady increase in the amplitude of scattered light (Figure 4). This threshold depends upon the specific time delay and generally it coincided with the evaporation threshold (shown by a dotted vertical line in Figure 4) when the fluence corresponding to the value of the bubble generation probability PRB (shown by a dashed line in Figure 4) was 0.5. In this case, the scattering relative amplitude K_{sc} begins to increase also almost linearly with the pump laser fluence, and the amplification effect ($K_{sc} > 1$) also increases with the time-delay of the probe pulse (Figure 5a). These two features of optical scattering at a higher pump laser fluence can be explained by the vapor bubble dynamics. At a specific level of the pump laser fluence the bubble diameter increases with time during its expansion stage (this can also be seen from Figure 3b) and so does the amplitude of the light scattered by the bubble.[27–30] The measured bubble lifetimes were in the 10–100 ns range (Figure 5b) so that the time delays of 0.5–9 ns definitely corresponded to the bubble expansion stage. At this stage, the longer the time delay, the bigger is the diameter of a bubble and, therefore, the higher is the amplitude of the light scattered.

Next, for the specific time-delay (specific temporal stage of bubble expansion) the bubble diameter increases with the initial pressure, which depends on the laser-induced initial temperature of the medium, and hence on the laser fluence. This explains the steady increase in the relative scattering amplitude K_{sc} with the fluence in Figure 4. When a bubble scatters the light, the amplitude of the scattered light is determined by the bubble diameter.[32,35–37] We could not measure this parameter directly, so we used the bubble lifetime (obtained through the time-response) as a measure of the bubble maximal diameter. Such an approach is justified as far as the maximal diameter of the bubble is proportional to its lifetime. We simultaneously measured the relative scattering amplitudes K_{sc} and the bubble lifetimes for the pump pulse fluences above the bubble generation thresholds and plotted the K_{sc} as a function of the bubble lifetime (Figure 5b). We can see a good correlation between these two parameters, and this confirms the above mechanism of the amplification of optical scattering around gold NPs by NP-generated bubbles.

Figures 4 and 5a show that at shortest delays of 0.5 and 1.5 ns the amplification effect does not occur even at high pump laser fluences, when the bubbles are generated around NPs, and the bleaching effect dominates the scattering. The explanation of this phenomenon also relates to the bubble dynamics. At such a stage, the bubble diameter (and hence its scattering power) is rather small because these times correspond to the very beginning of the bubble expansion (see also Figure 3b), and therefore the optical amplification effect due to the bubble is minimal. As a result, the bleaching effect dominates the scattering at early stage of heat transfer between an NP and its environment even despite a rather high fluence of a pump laser pulse.

The bubble generation around NPs has a threshold nature and besides was found to be NP size-dependent. In our experiments, the bubble generation threshold was the highest for 90 nm NPs (0.36 J/cm^2) and it was found to be lower for 250 nm NPs (0.18 J/cm^2); see Figure 4. In the previous studies of the laser-induced generation of vapor bubbles around gold NPs we also found that the pump laser fluence threshold for the bubble generation significantly decreased with the size of the NPs and in the case of their clusterization.[27,32,38] This and also the revealed optical properties of the NP-generated thermal effects suggest new approaches for improving the sensitivity and the contrast of scattering imaging with plasmonic NPs:

1. Identical NPs and a nonuniform pump laser beam: scattering will be amplified in the spatial maxima of the laser fluence and will be suppressed (bleached) in the areas corresponding to the lower fluence. The maximal fluence should exceed the evaporation threshold.
2. Identical NPs with the different states of aggregation (single NPs and their clusters) and a uniform pump beam at the fluence that is above the evaporation thresholds for NP clusters, but below the evaporation threshold for a single NP. The scattering around clusters of aggregated NPs will be amplified by the bubbles, while the scattering around single NPs will be suppressed (bleached).
3. NPs of different diameters and a uniform pump beam at the fluence that is above the evaporation thresholds for larger NPs but below the evaporation threshold for smaller NPs: The scattering around NPs of larger size will be amplified by the bubbles, while the scattering around small NPs will be suppressed (bleached).
4. NPs of identical sizes (and hence with similar scattering properties), but with different optical absorbance cross-sections (spheres and shells, for example) and a uniform pump beam at the fluence that is above the evaporation thresholds for NPs with a high absorbance cross-section, but below the evaporation threshold for NPs with a low absorbance cross-section: the scattering around NPs with the high absorbance will be amplified by the bubbles, while the scattering around NPs with the low absorbance will be suppressed (bleached).

Our experimental model and results were obtained for a specific time domain that is longer than the time scale for initial thermal processes in NPs[16,19,20] though much shorter than the time scale in many typical photothermal applications of gold NPs (from microseconds to minutes). Nevertheless, the influence of the environmental heating and evaporation on optical scattering may occur at much longer (up to continuous) photothermal interactions providing there are the temperature and phase gradients around scattering NPs. We have shown that optical scattering by NPs depends on the optical absorbance by NPs due the secondary photothermal processes in NP environment. The discovered optical effects are not directly related to the primary photothermal processes inside NPs but rather relate to the thermal interaction of NP with its nanoenvironment and include the two opposite effects that can be determined as transient environmental photothermal phenomena:

1. bleaching (suppression) of optical scattering by plasmonic NPs due to heating of the medium around them.
2. amplification of optical scattering by plasmonic NPs due to the generation of vapor bubbles around them.

The effects revealed demonstrated significant enhancement (more than 1 order of magnitude) of optical contrast for specific NPs and thus may improve the sensitivity and specificity of plasmonic NPs as optical probes. It should be noted that to the degree that the observed changes in scattering are due solely to the existence of refractive index gradients, a uniform thermal field will not influence the scattering. Therefore, the interaction of scattering and photothermal phenomena can take place only for localized photothermal inhomogeneities that create refractive index gradients. The major increase in the sensitivity of optical detection is provided by the NP-generated vapor bubbles that can be activated on-demand by a specific pump laser radiation and, unless activated, do not present in the sample.

Acknowledgments

The authors would like to thank Nina Yakush for her technical assistance with photothermal experiments. D. Lapotko acknowledges support from NIH 1R21CA133641 and from the Institute of International Education/SRF (New York, NY).

References

1. Sokolov K, Follen M, Aaron J, Pavlova I, Malpica A, Lotan R, Richards-Kortum R. Cancer Res 2003;63:1999–2004. [PubMed: 12727808]
2. Yguerabide J, Yguerabide E. Anal Biochem 1998;262:157–176. [PubMed: 9750129]
3. Javier D, Nitin Nitin, Roblyer D, Richards-Kortum R. J Nanophoton 2008;2:023506.
4. Hu Y, Fleming R, Drezek R. Opt Express 2008;16:19579–19591. [PubMed: 19030045]
5. Liao H, Nehl C, Hafner J. Nanomedicine 2006;1:201–208. [PubMed: 17716109]
6. Jingyi, Chen; Fusayo, Saeki; Wiley, B.; Hu, Cang; Cobb, M.; Zhi-Yuan, Li; Au, L.; Hui, Zhang; Kimmey, M.; Xingde, Li; Younan, Xia. Nano Lett 2005;5:473–477. [PubMed: 15755097]
7. El-Sayed IH, Huang X, El-Sayed MA. Nano Lett 2005;5:829–834. [PubMed: 15884879]
8. van Dijk M, Tchebotareva A, Orrit M, Lippitz M, Berciaud S, Lasne D, Cognetc L, Louni B. Phys Chem Chem Phys 2006;8:3486–3495. [PubMed: 16871337]
9. Pitsillides M, Joe E, Wei X, Anderson R, Lin C. Biophys J 2003;84:4023–4032. [PubMed: 12770906]
10. Loo C, Lowery A, Halas N, West J, Drezek R. Nano Lett 2005;5:709–711. [PubMed: 15826113]
11. Tong L, Zhao Y, Huff T, Hansen M, Wei A, Cheng J. Adv Mater 2007;19:3136–3141.
12. Yao C, Rahmanzadeh R, Endl E, Zhang Z, Gerdes J, Huttmann G. J Biomed Opt 2005;10:064012. [PubMed: 16409077]
13. El-Sayed I, Huang X, El-Sayed M. Cancer Lett 2006;239:129–135. [PubMed: 16198049]
14. Govorov O, Richardson H. Nano Today 2007;1:30–38.

15. Otter M. Z Phys 1961;161:539–549.
16. Hu M, Hartland G. Chem Phys Lett 2004;391:220–225.
17. Plech A, Cerna R, Kotaidis V, Hudert F, Bartels A, Dekorsy T. Nano Lett 2007;13:17352505.
18. Inasawa S, Sugiyama M, Noda S, Yamaguchi Y. J Phys Chem B 2006;110:3114–3119. [PubMed: 16494317]
19. Petrova H, Min H, Hartland G. Z Phys Chem 2007;221:361–376.
20. Hu M, Hartland G. J Phys Chem B 2002;106:7029–7033.
21. Kotaidis V, Dahmen C, von Plessen G, Springer F, Plech A. J Chem Phys 2006;124:184702. [PubMed: 16709126]
22. Farny H, Wu T, Holt R, Murray T, Roy R. Acoust Res Lett Online 2005;6:138–143.
23. François L, Mostafavi M, Belloni J, Delaire. J Phys Chem 2001;3:4965–4971.
24. Hu M, Chen J, Zhi-Yuan Li, Au L, Hartland G, Xingde Li, Marqueze M, Younan X. Chem Soc Rev 2006;35:1084–1094. [PubMed: 17057837]
25. Moller, R.; Fritzsche, W. Annual review of nano research. Cao, G.; Brinker, CJ., editors. World Scientific Publishing Co. Pte. Ltd.; Hackensack, NJ: 2007. p. 429-444.
26. Lapotko D, Lukianova E, Shnip A. J Biomed Opt 2005;10:014006.
27. Lapotko D. Opt Express 2009;17:2538–2556. [PubMed: 19219157]
28. Hleb E, Lapotko D. Nanotechnology 2008;19:355702.
29. Vogel A, Noack J, Hüttmann G, Paltauf G. Appl Phys B 2005;81:1015–1047.
30. Rayleigh L. Philos Mag 1917;34:94–98.
31. Brennen, CE. Cavitation and bubble dynamics. Oxford University Press, Oxford Engineering Science; New York: 1995. p. 44
32. Hleb E, Ying Hu, Drezek R, Hafner J, Lapotko D. Nanomedicine 2008;3:797–812. [PubMed: 19025454]
33. Mie G. Ann Phys 1908;25:377–445.
34. Yguerabide O, Yguerabideb E. Anal Biochem 1998;262:137–156. [PubMed: 9750128]
35. Yavas O, Leiderer P, Park H, Grigoropoulos C, Poon C, Leung W, Nhan Do, Tam A. Phys Rev Lett 1993;70:1830–1833. [PubMed: 10053397]
36. Kokhanovsky A. J Opt A: Pure Appl Opt 2003;5:47–52.
37. Vogel A, Linz N, Freidank S, Paltauf G. Phys Rev Lett 2008;100:038102. [PubMed: 18233040]
38. Lapotko D, Lukianova-Hleb E, Oraevsky A. Nanomedicine 2007;2:241–253. [PubMed: 17716124]

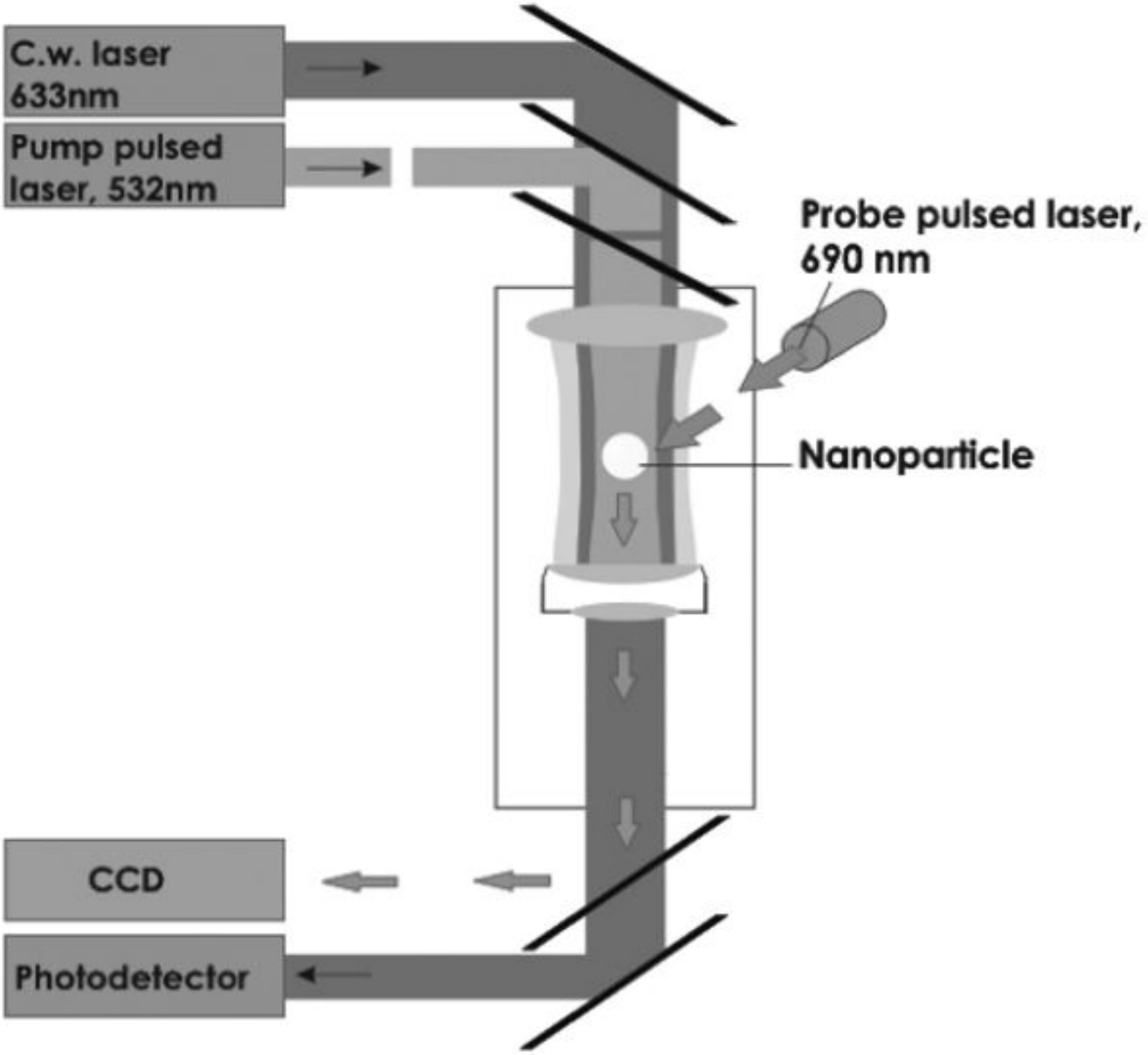

Figure 1.
Experimental setup: individual gold nanoparticles are coaxially illuminated by a pump laser pulse (532 nm), by a continuous probe laser (633 nm), and also by a probe laser pulse (690 nm). Probe radiation was detected by a CCD camera and a photodetector.

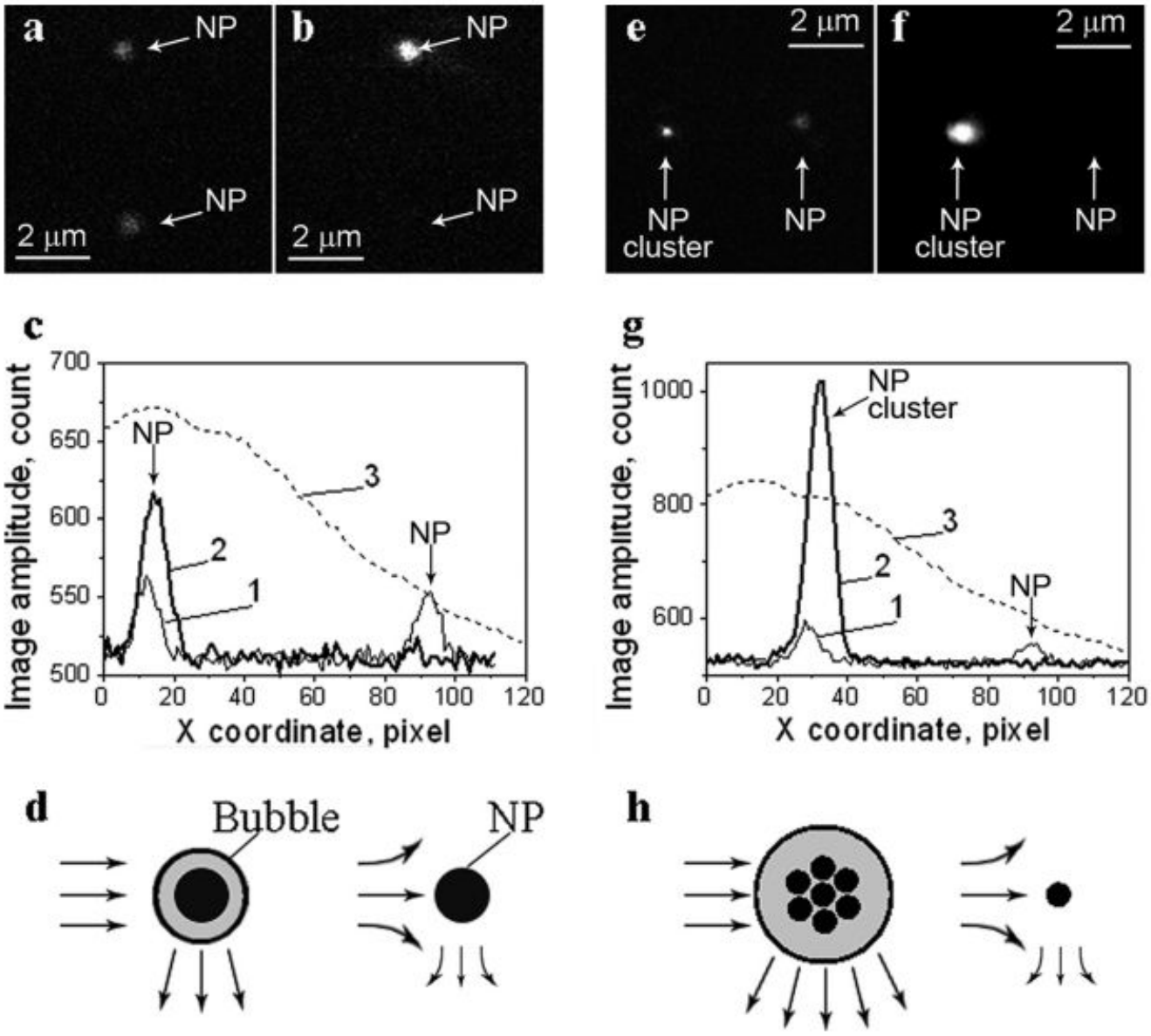

Figure 2.

Optical scattering time-resolved images of gold spheres; left panel (a,b)—a pair of identical 250 nm gold NPs, right panel (e,f)—a pair of a single 90 nm NPs and a cluster of 90 nm NPs; (a) and (e)—pulsed scattering images obtained without a pump pulse; (b) and (f)—pulsed scattering images obtained at a delay of 9 ns after the pump pulse (532 nm, 0.5 ns); (c) and (g)—the spatial profiles of the pump beam fluence show the difference in the irradiation of two NPs (3) and of the image pixel amplitudes for the images shown in (a), (b), (e), and (f), respectively: 1—scattering signal amplitude obtained without a pump pulse corresponds to (a) and (e), 2—scattering signal amplitude obtained with a pump pulse corresponds to (b) and (f); (d) and (h)—the schemes illustrating the possible mechanisms of thermal influence on scattering during evaporation (the bubble amplifies the scattering) and heating (the scattering of the probe beam by the thermal gradients of the refractive index of the NP environment) of the NP environment.

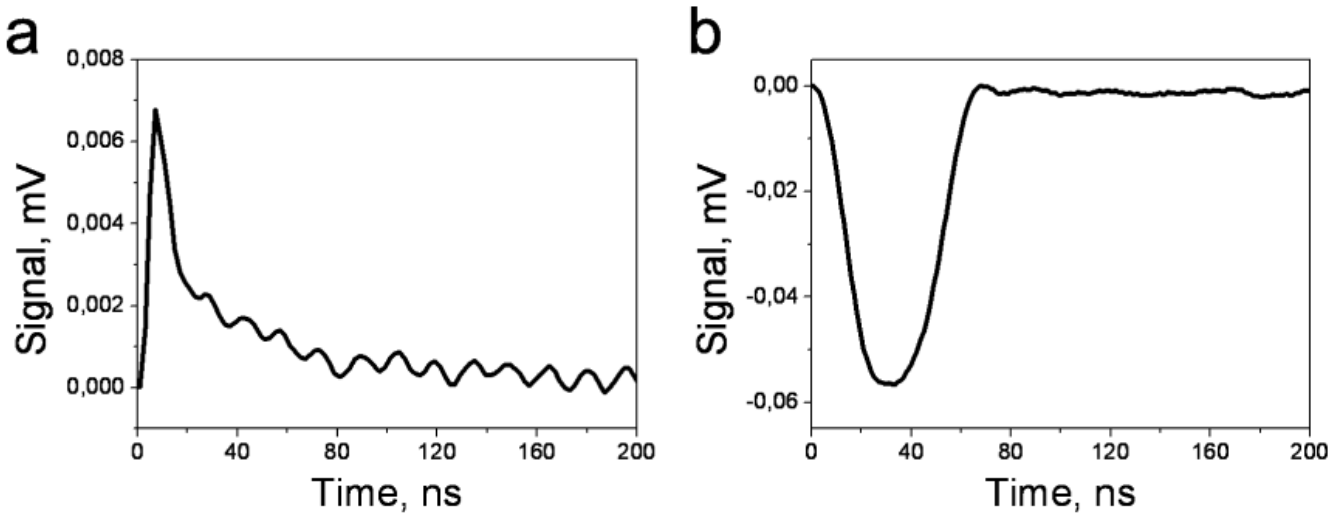

Figure 3.

Photothermal integral time responses of the 90 nm NP suspension as registered by a continuous probe laser beam during the application of a single pump pulse (532 nm, 0.5 ns): (a) fast heating and slow cooling of the suspension at a pump pulse fluence of 0.08 J/cm^2 and below evaporation threshold; (b) bubble-specific signal of the opposite sign that shows the expansion and the collapse, a pump pulse fluence of 0.4 J/cm^2 is above the evaporation threshold. The ripple patterns were caused by the probe laser noise, and the *x* coordinate indicates the time from the moment of exposure of NPs to a pump laser pulse.

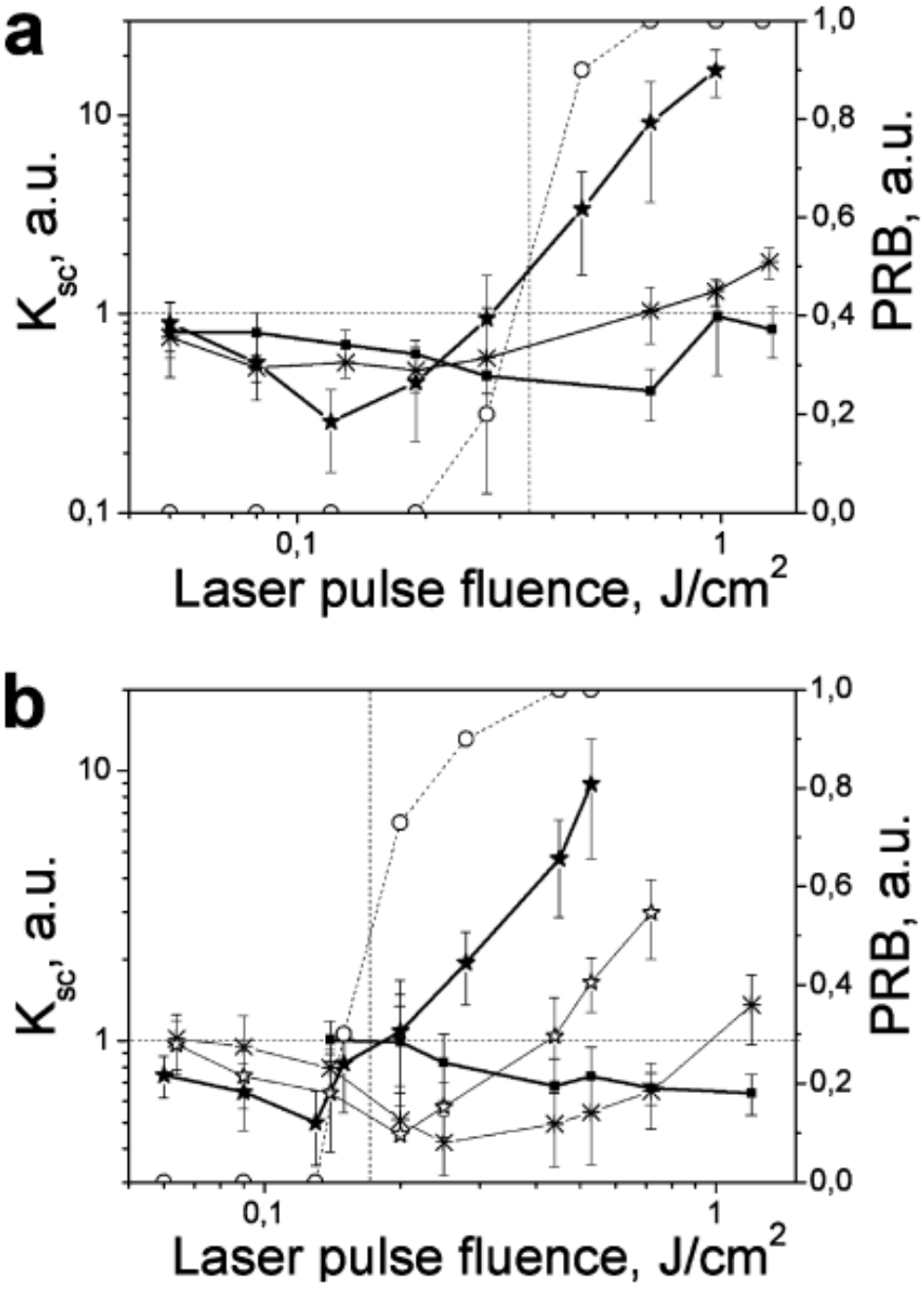

Figure 4.
Relative scattering efficacy of individual NPs ((a) for 90 NPs; (b) for 250 nm NPs), K_{sc} measured as a function of the pump pulse fluence at several time delays between the pump and probe pulses: solid square at 0.5 ns; snowflake at 1.5 ns; hollow star at 2.5 ns; solid star at 9 ns; hollow circle and the dotted line shows the probability PRB of the bubble generation around an NP as independently measured by the thermal lens method.

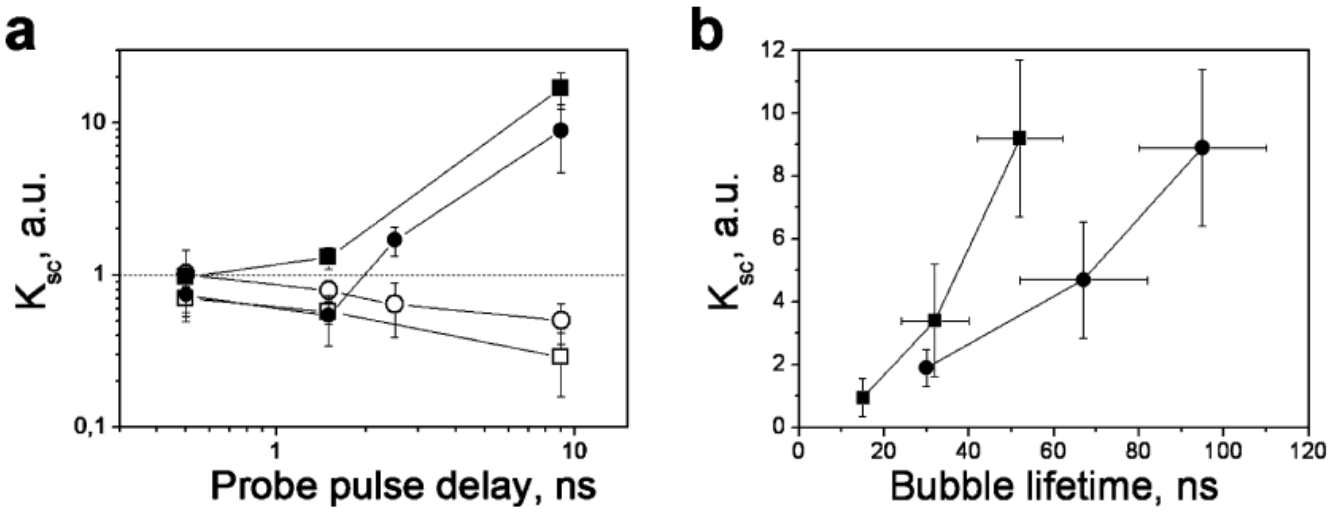

Figure 5.

Relative scattering efficacy K_{sc} of individual 90 nm and 250 nm NPs as a function of (a) the time delay between the probe and pump pulses obtained at pump fluence level below (□, 90 nm; ○, 250 nm) and above (■, 90 nm; ●, 250 nm) the evaporation thresholds and (b) the bubble lifetime (obtained for 90 nm (■) and 250 nm (●) NPs (the delay of the probe pulse was 9 ns) and at the pump fluences above the evaporation threshold).